

Radiation Zeros in High-Energy e^+e^- Annihilation into Hadrons

M. Heyssler^a and W.J. Stirling^{a,b}

^a *Department of Physics, University of Durham, Durham, DH1 3LE*

^b *Department of Mathematical Sciences, University of Durham, Durham, DH1 3LE*

Abstract

The process $e^+e^- \rightarrow q\bar{q}\gamma$ contains radiation zeros, i.e. configurations of the four-momenta for which the scattering amplitude vanishes. We calculate the positions of these zeros for u -quark and d -quark production and assess the feasibility of identifying the zeros in experiments at high energies. The radiation zeros are shown to occur also for massive quarks, and we discuss how the $b\bar{b}\gamma$ final state may offer a particularly clean environment in which to observe them.

1 Introduction

In certain high-energy scattering processes involving charged particles and the emission of one or more photons, the scattering amplitude vanishes for particular configurations of the final-state particles. Such configurations are known as *radiation zeros* or *null zones*. A very clear and comprehensive review by Brown can be found in Ref. [1].

Radiation zeros have an interesting history. Although they are in principle present in QED amplitudes, they first attracted significant attention in processes involving weak bosons. For example, the pioneering papers of Mikaelian, Sahdev and Samuel [2] and Brown, Sahdev and Mikaelian [2] considered radiative charged weak boson production in $q\bar{q}$ and νe collisions. The cross sections for these processes vanish when the photon is emitted in certain directions (see below). Recently, experimental evidence for zeros of this type has been found at the Fermilab Tevatron $p\bar{p}$ collider [4]. In addition to the phenomenological analyses, a deeper theoretical understanding was developed in the papers of Ref. [5]: the vanishing of the (tree-level) scattering amplitude can be understood as arising from complete destructive interference of the classical radiation patterns of the incoming and outgoing charged particles.

There have been many other studies exploring the phenomenological aspects of radiation zeros. For example, the introduction of (non-gauge) ‘anomalous couplings’ destroys the cancellation which leads to the vanishing of the amplitude, and so radiation zeros can be used as sensitive probes of new physics [6–8]. More recently, the possibility of detecting radiation zeros in eq scattering at HERA has been investigated [9–13].

In the course of analysing the $eq \rightarrow eq\gamma$ matrix elements for ‘standard’ radiation zeros in Ref. [13], a new type of zero was discovered. This appears to arise in a wider class of processes, and in particular in the crossed process $e^+e^- \rightarrow q\bar{q}\gamma$. This opens up the possibility of identifying radiation zeros in high-energy e^+e^- annihilation into hadrons, for example at a future linear collider. The purpose of the present study is to calculate the position of these zeros and to assess the feasibility of their observation in experiment.

Before studying the e^+e^- annihilation process in detail, it may be useful to make some general observations on the various types of radiation zeros. The discussion is particularly simple when one considers the amplitude for the emission of a single soft photon in a scattering process $1 + 2 \rightarrow 3 + 4 + \dots$ involving charged particles.

The matrix element for one (soft) photon emission can be written as

$$\mathcal{M}_\gamma \simeq eJ \cdot \epsilon \mathcal{M}_0, \quad (1)$$

where \mathcal{M}_0 is the leading-order (no photon emission) matrix element and ϵ is the polarisation vector of the photon, with polarisation and helicity labels suppressed for the moment. The current is given by

$$J^\mu = \sum_i e_i \eta_i \frac{p_i^\mu}{p_i \cdot k}, \quad (2)$$

where e_i is the charge of the i th particle and $\eta_i = +1, -1$ for incoming, outgoing particles. Energy-momentum and charge conservation give $\sum_i \eta_i p_i^\mu = 0$ and $\sum_i e_i \eta_i = 0$ respectively.

The classical (type 1) radiation zeros are obtained by noting that the condition

$$\frac{e_i}{p_i \cdot k} = \kappa, \quad (3)$$

where κ is a constant independent of i , immediately yields $J^\mu = 0$ and hence $\mathcal{M}_\gamma = 0$, for all helicities and polarisations. Note that type 1 zeros require all particles to have the same sign of electric charge. A simple example is provided by $u(p_1) + \bar{d}(p_2) \rightarrow W^+(p_3) + \gamma(k)$, where a zero of the amplitude is obtained for

$$\frac{2}{3} \frac{1}{p_1 \cdot k} = \frac{1}{3} \frac{1}{p_2 \cdot k} \quad \Rightarrow \quad \cos \theta_\gamma = -\frac{1}{3}, \quad (4)$$

where θ_γ is the polar angle of the photon in the c.m.s. frame with $\theta_\gamma = 0^\circ$ in the incoming u -quark direction.

Type 2 zeros, on the other hand, only arise when the scattering is *planar* [13], i.e. the three-momenta of all the particles including the photon lie in the same plane. In this case, if one chooses one of the photon polarisation vectors ϵ_\perp to be orthogonal to the scattering plane then $\epsilon_\perp \cdot p_i = 0$ for all i gives $\epsilon_\perp \cdot J = 0$ for *any* orientation of the particles and photon in the plane. The requirement that the amplitude vanishes for *all* helicities and polarisations means that one must also have $\epsilon_\parallel \cdot J = 0$, where (the spatial part of) ϵ_\parallel^μ is in the scattering plane and orthogonal to the photon direction. The solution of $\epsilon_\parallel \cdot J = 0$ then gives the position in photon angular phase of the radiation zero. If we denote the direction of the three-momentum of particle i by \vec{n}_i and the direction of the photon by \vec{n} , then the condition is (for massless particles)

$$\sum_i e_i \eta_i \frac{\vec{\epsilon}_\parallel \cdot \vec{n}_i}{1 - \vec{n} \cdot \vec{n}_i} = 0, \quad (5)$$

with $\vec{\epsilon}_\parallel \cdot \vec{n} = 0$. After some algebra, Eq. (5) can be cast into the simpler form

$$\sum_i e_i \eta_i \cot(\theta_{\gamma i}/2) = 0, \quad (6)$$

where $\theta_{\gamma i}$ is the angle between the photon and particle i directions.¹ Eq. (6) allows us to derive an existence proof for the zeros. First we note that $\cot(\theta_{\gamma i}/2) \rightarrow \infty$ as $\theta_{\gamma i} \rightarrow 0$ — these are the usual collinear singularities for massless gauge boson emission from massless fermions. Second, we note that not all the $e_i \eta_i$ can have the same sign (charge conservation). Therefore there exists at least one angular sector, between j and k say, where the collinear singularity has the opposite sign (i.e. $\rightarrow \pm\infty$) on the boundaries of the sector. Since the left-hand side of (6) defines a continuous function of the photon polar angle away from the collinear singularities, according to the Intermediate Value Theorem the function must vanish somewhere in the sector between j and k . The exact location of the zero depends not only on the strength of the collinear singularities at $\theta_{\gamma j}, \theta_{\gamma k} = 0$ but also on the other non-singular contributions ($i \neq j, k$) to the current in that region.

For $2 \rightarrow 2$ scattering the solutions to (5) or (6) can be found analytically, for more complicated scattering numerical methods can be used. The existence of zeros requires certain constraints on the charges, masses and scattering kinematics to be satisfied, as we shall see in the following sections. For example, there are no collinear singularities for massive fermions, and therefore the existence of a radiation zero in the angular sector depends on how strongly the distribution is peaked close to the massive particles, which in turn depends on the exact value of the mass.

¹Note that $\theta_{\gamma i}$ must be defined in the same sense (clockwise or anticlockwise from the γ direction) for each particle, so that the cot can have either sign.

Type 2 zeros do not require that all the charges have the same sign. For example, the process $e^-d \rightarrow e^-d\gamma$ has zeros of both types, whereas $e^-e^+ \rightarrow d\bar{d}\gamma$ only has type 2 zeros (see below). Although for simplicity we have used soft-photon matrix elements and kinematics in the discussion above, radiation zeros of both types are also found when exact kinematics and matrix elements are used [13].

In this paper we present a detailed theoretical and phenomenological study of (type 2) radiation zeros in the scattering process $e^-e^+ \rightarrow q\bar{q}\gamma$ at high energy. We shall show that zeros exist for both u - and d -type quarks for all helicities and polarisations. The zeros occur in photon directions which are reasonably well separated from the directions of the other particles in the scattering. Unfortunately it is very difficult to obtain analytic expressions for the positions of the zeros with exact matrix elements and phase space. Results for the general case, obtained numerically, will be presented in Section 5. However in the soft-photon approximation (which in fact is the dominant experimental configuration) it is possible to obtain reasonably compact expressions. In Sections 2 and 4 we use the soft-photon approximation to locate the zeros, first for massless and then for massive quarks. Section 3 briefly discusses radiation at the Z pole. In Section 6 we perform a Monte Carlo study, based on the exact matrix elements and phase space, to obtain ‘realistic’ distributions of the type which might be accessible experimentally. Finally, our conclusions are presented in Section 7.

2 Massless quarks in the soft limit

We consider the processes

$$e^-(1) e^+(2) \longrightarrow q(3) \bar{q}(4) + \gamma(k), \quad (7)$$

$$e^-(1) e^+(2) \longrightarrow q(3) \bar{q}(4) + g(k). \quad (8)$$

The gluon emission process (8) does *not* contain radiation zeros, but is useful for comparison. To begin with we shall consider s -channel γ^* exchange only, as this fully determines the positions of the radiation zeros. The exact matrix elements for these processes are (for massless quarks and leptons, see for example Ref. [14])

$$|\overline{\mathcal{M}}_3|^2(e^-e^+ \rightarrow q\bar{q} + \gamma) = -3e^6 e_q^2 \frac{t^2 + t'^2 + u^2 + u'^2}{ss'} (v_{12} + e_q v_{34})^2, \quad (9)$$

$$|\overline{\mathcal{M}}_3|^2(e^-e^+ \rightarrow q\bar{q} + g) = -4e^4 e_q^2 g_s^2 \frac{t^2 + t'^2 + u^2 + u'^2}{ss'} (v_{34})^2, \quad (10)$$

with the standard definitions for the $2 \rightarrow 3$ Mandelstam variables

$$\begin{aligned} s &= (p_1 + p_2)^2, & t &= (p_1 - p_3)^2, & u &= (p_1 - p_4)^2, \\ s' &= (p_3 + p_4)^2, & t' &= (p_2 - p_4)^2, & u' &= (p_2 - p_3)^2, \end{aligned} \quad (11)$$

and

$$v_{ij} = \frac{p_i^\mu}{p_i \cdot k} - \frac{p_j^\mu}{p_j \cdot k}. \quad (12)$$

In the soft limit, i.e. $\omega_{\gamma,g}/E_i \rightarrow 0$, we may use $2 \rightarrow 2$ kinematics for the $e^-e^+ \rightarrow q\bar{q}$ part of the process. The four-vectors in the c.m.s. frame can then be written as

$$p_1^\mu = \frac{\sqrt{s}}{2} (1, 0, 0, -1), \quad (13)$$

$$p_2^\mu = \frac{\sqrt{s}}{2} (1, 0, 0, 1), \quad (14)$$

$$p_3^\mu = \frac{\sqrt{s}}{2} (1, -\sin \Theta_{\text{cm}}, 0, -\cos \Theta_{\text{cm}}), \quad (15)$$

$$p_4^\mu = \frac{\sqrt{s}}{2} (1, \sin \Theta_{\text{cm}}, 0, \cos \Theta_{\text{cm}}), \quad (16)$$

$$k^\mu = \omega_{\gamma,g} (1, \sin \theta_{\gamma,g} \cos \phi_{\gamma,g}, \sin \theta_{\gamma,g} \sin \phi_{\gamma,g}, \cos \theta_{\gamma,g}). \quad (17)$$

These kinematics are illustrated in Fig. 1.

Radiation zeros for process (7) arise from the vanishing of the $(v_{12} + e_q v_{34})^2$ term. This is the ‘antenna pattern’ $\mathcal{F}^\gamma = -J \cdot J$ of the soft emission process, see for example Refs. [15–17]. A useful parameterisation is to introduce the variables $z_i = \cos \theta_i$ which specify the angular separation of the soft photon or gluon from particle i . The eikonal factors which make up the antenna pattern are then

$$[ij] \equiv \frac{p_i \cdot p_j}{(p_i \cdot k)(p_j \cdot k)} = \frac{1}{\omega^2} \frac{1 - \cos \theta_{ij}}{(1 - z_i)(1 - z_j)}, \quad (18)$$

and the antenna patterns themselves can be readily obtained from Eqs. (9,10)

$$\frac{1}{2} \mathcal{F}^\gamma = [12] + e_q^2 [34] - e_q ([13] + [24] - [14] - [23]), \quad (19)$$

$$\frac{1}{2} \mathcal{F}^g = [34]. \quad (20)$$

We see immediately that there are no radiation zeros of type 1 [13], as this would require (for the vanishing of \mathcal{F}^γ)

$$\frac{-1}{1 + z_2} = \frac{1}{1 - z_2} = \frac{e_q}{1 + z_4} = \frac{-e_q}{1 - z_4}, \quad (21)$$

which has no solutions in the physical domain.

In contrast, type 2 radiation zeros are located in the event scattering plane [13] and do *not* fulfill condition (21). For a complete set of kinematic variables in the soft-photon limit we may take the $q\bar{q}$ c.m.s. scattering angle Θ_{cm} and two of the z_i variables introduced above: $\mathcal{F}^\gamma = \mathcal{F}^\gamma(\Theta_{\text{cm}}, e_q, z_2, z_4)$, since $z_1 = -z_2$ and $z_3 = -z_4$ in the c.m.s. frame. To locate the zeros we solve

$$\mathcal{F}^\gamma(\Theta_{\text{cm}}, e_q, z_2, z_4) = 0 \quad (22)$$

and find

$$\hat{z}_4 = -e_q z_2 \pm \sqrt{f(\Theta_{\text{cm}}, e_q)}, \quad (23)$$

with

$$f(\Theta_{\text{cm}}, e_q) = 1 + e_q^2 + 2e_q \cos \Theta_{\text{cm}}. \quad (24)$$

As we expect the (type 2) radiation zeros to be located in the scattering plane,² we set $\phi_\gamma = 0^\circ$ and derive as an additional condition

$$\begin{aligned} z_4 = \cos \theta_4 &= \cos(\theta_\gamma - \Theta_{\text{cm}}) = \sin \theta_\gamma \sin \Theta_{\text{cm}} + \cos \theta_\gamma \cos \Theta_{\text{cm}} \\ &= \sqrt{1 - z_2^2} \sin \Theta_{\text{cm}} + z_2 \cos \Theta_{\text{cm}}. \end{aligned} \quad (25)$$

The solutions of Eqs. (23) are tangential hyperplanes to Eq. (25) in the Θ_{cm}, z_2 space for given charge e_q . Thus we find the positions of the radiation zeros for given e_q and c.m.s. scattering angle by solving

$$\frac{d}{dz_2} \hat{z}_4 = \frac{d}{dz_2} \left(\sqrt{1 - z_2^2} \sin \Theta_{\text{cm}} + z_2 \cos \Theta_{\text{cm}} \right), \quad (26)$$

which immediately yields

$$e_q = \frac{z_2}{\sqrt{1 - z_2^2}} \sin \Theta_{\text{cm}} - \cos \Theta_{\text{cm}}. \quad (27)$$

The solutions are

$$\hat{z}_2 = \cos \hat{\theta}_\gamma = \pm \frac{e_q + \cos \Theta_{\text{cm}}}{\sqrt{f(\Theta_{\text{cm}}, e_q)}}, \quad (28)$$

with ‘+’ if $\hat{\phi}_\gamma = 0^\circ$ and ‘-’ if $\hat{\phi}_\gamma = 180^\circ$. Eq. (28) yields physical solutions for both $e_q = -1/3$ (d -type quarks) and $e_q = 2/3$ (u -type quarks) in the complete range of Θ_{cm} .

We mention several other interesting features.

- (i) If we substitute the solution for \hat{z}_2 of Eq. (28) and \hat{z}_4 of Eq. (23) into the antenna pattern \mathcal{F}^γ we find

$$[12] = e_q^2 [34] = \frac{1}{2} e_q ([13] + [24] - [14] - [23]), \quad (29)$$

i.e. the interference term exactly cancels the sum of the leading pole terms which are equal. Therefore solving $\mathcal{F}^\gamma = 0$ is equivalent to solving $[12] = e_q^2 [34]$ in the massless case. We shall test this feature later for massive quarks.

- (ii) From Eq. (28) we see that the radiation zeros are orthogonal to the beam direction for $\cos \Theta_{\text{cm}} = -e_q$ which means $\Theta_{\text{cm}} \sim 131.8^\circ$ for u -type quarks and $\Theta_{\text{cm}} \sim 70.5^\circ$ for d -type quarks.
- (iii) The radiation zeros are located in different sectors: for d -type quarks they are located between the directions of the incoming e^+ and outgoing \bar{q} and between the incoming e^- and outgoing q directions, respectively. For u -type quarks the radiation zeros can be found between the incoming e^- and outgoing \bar{q} and between the incoming e^+ and outgoing q directions, respectively. This makes the discrimination between different charged quarks straightforward, at least in principle.

²Note that it is straightforward to show that there are no additional zeros with $\phi_\gamma \neq 0^\circ, 180^\circ$.

- (iv) There is one kinematic configuration for which the separation between the radiation zero direction and the direction of the outgoing quark (antiquark) is maximal. By solving

$$\frac{d}{d\Theta_{\text{cm}}} \left\{ \cos^{-1} \left(\pm \frac{e_q + \cos \Theta_{\text{cm}}}{\sqrt{f(\Theta_{\text{cm}}, e_q)}} \right) - \Theta_{\text{cm}} \right\} = 0, \quad (30)$$

we can show that this is the case if the radiation zeros are located *orthogonal* to the beam direction (the corresponding values of Θ_{cm} are given above). The separations are then

$$\Delta\theta_{\gamma}^{\text{max}} = 41.8^{\circ} \quad \text{for } u\text{-type quarks}, \quad (31)$$

$$\Delta\theta_{\gamma}^{\text{max}} = 19.5^{\circ} \quad \text{for } d\text{-type quarks}. \quad (32)$$

In Figs. 2,3 we show the antenna patterns \mathcal{F}^{γ} of Eq. (19) for process (7) with three different c.m.s. frame scattering angles $\Theta_{\text{cm}} = 60^{\circ}, 90^{\circ}$ and 120° . Additionally we show a slice through the soft-photon phase space at $\hat{\phi}_{\gamma} = 0^{\circ}$ to illustrate the positions of the radiation zeros. For comparison we also show the antenna patterns for soft-gluon emission as defined in Eq. (20). This has no initial-, final-state interference and therefore no zeros.³ Comparing the production of d -type quarks and u -type quarks, i.e. Figs. 2 and 3, shows that the most striking qualitative feature is the appearance of radiation zeros in different sectors, as discussed above.

In Fig. 4 we present the positions of the radiation zeros ($\hat{\phi}_{\gamma} = 0^{\circ}, \hat{\theta}_{\gamma}$) given by Eq. (28), as a function of the c.m.s. frame scattering angle, for both d -type and u -type quarks. Note that radiation zeros exist in both cases for all values of Θ_{cm} , and also that the radiation zeros for u -type production are more clearly separated from the collinear singularities. For zero-angle scattering ($\Theta_{\text{cm}} = 0^{\circ}, 180^{\circ}$) the zeros become pinched along the beam direction. Note that the t -channel process $e^+q \rightarrow e^+q\gamma$ [13] shows a qualitatively different behaviour in the zero-angle scattering limit: in that case the radiation zeros were located on a cone with fixed angle around the beam direction.

It should be obvious from the above that in order to locate a radiation zero one has to be able to distinguish a quark jet from an antiquark jet. Thus if one ($3 \leftrightarrow 4$) symmetrises the expression in Eq. (19) for \mathcal{F}^{γ} , the interference term vanishes and there is no zero. In practice distinguishing between the quark and antiquark jet is likely to be very difficult, but not impossible. For example, for light-quark jets one could try to tag on the charge of the fastest hadron in the jet. For heavy (charm, bottom) quark jets one could in principle use the charge of the lepton from the primary weak decay of the quark to distinguish the quark from the antiquark. Methods like these are likely to have poor efficiency, so in practice one would be looking for a slight dip in the photon distribution in the vicinity of a zero when a tagged sample is compared with an untagged sample with the same overall kinematics.

3 Radiation on the Z^0 pole

The general discussion on radiation zeros presented in the Introduction assumed that the hard scattering is characterised by a single (large) energy scale, so that the incoming and

³Note that up to charge factors the final-state collinear singularities are the same in both cases however.

outgoing particles emit photons on the same timescale. This corresponds to coherent emission and allows the interference to be maximal. However, care must be taken when two timescales are involved, for example when there is an intermediate particle which is relatively long lived. In this case the emission off the initial- and final-state particles can occur at very different timescales and the interference between them can be suppressed. In fact this is exactly what happens for the process $e^+e^- \rightarrow f\bar{f}$ on the Z pole, i.e. when $\sqrt{s} \simeq M_Z$.

A formalism has been developed for taking these effects into account (see Refs. [15 – 22] and in particular Ref. [20]). In simple terms, the interference between emission during the production and decay stages of a heavy unstable resonance of width Γ is suppressed by a factor $\chi = \Gamma^2/(\Gamma^2 + \omega^2)$, i.e. there can be no interference when the timescale for photon emission ($\sim 1/\omega$) is much shorter than the lifetime of the resonance ($\sim 1/\Gamma$).

In the present context, the antenna pattern of Eq. (19) is only valid far away from the Z pole, $\sqrt{s} \ll M_Z$ or $\sqrt{s} \gg M_Z$. On the Z pole we have, in contrast,

$$\frac{1}{2}\mathcal{F}_Z^\gamma = [12] + e_q^2[34] - \chi_Z e_q ([13] + [24] - [14] - [23]) , \quad (33)$$

where

$$\chi_Z = \frac{M_Z^2 \Gamma_Z^2}{(P_Z \cdot k)^2 + M_Z^2 \Gamma_Z^2} = \frac{\Gamma_Z^2}{\omega^2 + \Gamma_Z^2} . \quad (34)$$

The second expression in (34) corresponds to the c.m.s. frame. For $\omega \gg \Gamma_Z$ there is no interference (and therefore no radiation zero), and the radiation pattern corresponds to incoherent emission off the initial- and final-state particles. On the other hand the radiation zero reappears in the limit $\omega/\Gamma_Z \rightarrow 0$. It is straightforward to show that in this limit the minimum value of the distribution is $\mathcal{O}(\omega^2/\Gamma_Z^2)$.

The effect of the finite Z width on the interference between initial- and final-state radiation was studied in detail in Ref. [23]. The DELPHI collaboration [24] subsequently confirmed the theoretical expectations and used the size of the measured interference to determine Γ_Z .

Since in the present study we are interested in radiation *zeros*, we must require that the collision energy (and the photon energy⁴) are such that the internal Z propagator is always far off mass-shell. This effectively guarantees that $\chi = 1$ and hence that the radiation pattern is again given by Eq. (19). Unfortunately this means that we are unable to use the greatly enhanced statistics of LEP1 and SLC in searching for radiation zeros.

4 Massive quarks in the soft photon limit

In this section we repeat the analysis of Section 2 but now including a non-zero mass for the final-state quarks. It is straightforward to derive the corresponding antenna pattern in the soft-photon approximation, see for example Refs. [17,20–22]. The eikonal factors for massive particles read

$$[ij]_m = \frac{1}{\omega^2} \frac{1 - \rho_i \rho_j \cos \theta_{ij}}{(1 - z_i \rho_i)(1 - z_j \rho_j)} . \quad (35)$$

⁴For $\sqrt{s} > M_Z$ we can avoid ‘radiative return’ to the Z pole by placing an upper bound on the photon energy.

We continue to use massless initial-state electrons, so that $\rho_1 = \rho_2 = 1$ and $\rho_3 = \rho_4 = \rho = \sqrt{1 - 4m_q^2/s}$. The antenna pattern of Eq. (19) now has additional contributions:

$$\begin{aligned} \frac{1}{2}\mathcal{F}_{m_q}^\gamma &= [12]_{m_q} + e_q^2 \left([34]_{m_q} - \frac{1}{2} \frac{m_q^2}{(p_3 \cdot k)^2} - \frac{1}{2} \frac{m_q^2}{(p_4 \cdot k)^2} \right) \\ &\quad - e_q \left([13]_{m_q} + [24]_{m_q} - [14]_{m_q} - [23]_{m_q} \right). \end{aligned} \quad (36)$$

We first consider the limits of $\rho \in [0, 1]$

$$\rho = 0 : \quad \mathcal{F}_{m_q}^\gamma = 2[12]_{m_q} = \frac{4}{\omega_\gamma^2} \frac{1}{1 - \cos^2 \theta_\gamma}, \quad (37)$$

$$\rho = 1 : \quad \mathcal{F}_{m_q}^\gamma = \mathcal{F}^\gamma. \quad (38)$$

The first of these limits is just the well-known result that heavy charged particles at rest do not radiate, and there are clearly no radiation zeros. As \mathcal{F}^γ does contain radiation zeros, we might anticipate a non-trivial ρ dependence of their position as we increase the mass from zero, with the zeros eventually vanishing for some critical mass.

A numerical study confirms this result. We again find zeros in the scattering plane ($\phi_\gamma = 0^\circ$). Solving $\mathcal{F}_{m_q}^\gamma = 0$ now gives

$$\hat{z}_2^{m_q} = \frac{2}{e_q} \frac{e_q \rho \cos \Theta_{\text{cm}} + 1 + \frac{g_\rho(\Theta_{\text{cm}}, e_q)}{2f_\rho(\Theta_{\text{cm}}, e_q)}}{\sqrt{-2f_\rho(\Theta_{\text{cm}}, e_q)g_\rho(\Theta_{\text{cm}}, e_q)}}, \quad (39)$$

with

$$f_\rho(\Theta_{\text{cm}}, e_q) = \rho^2 + e_q^2 + 2e_q \rho \cos \Theta_{\text{cm}}, \quad (40)$$

$$h_\rho(\Theta_{\text{cm}}, e_q) = -2e_q \cos \Theta_{\text{cm}} (1 + \rho^2) - \rho e_q^2 (1 + \cos^2 \Theta_{\text{cm}}) - 2\rho, \quad (41)$$

$$g_\rho(\Theta_{\text{cm}}, e_q) = \rho h_\rho(\Theta_{\text{cm}}, e_q) + \rho \sqrt{h_\rho(\Theta_{\text{cm}}, e_q)^2 - 4f_\rho(\Theta_{\text{cm}}, e_q) (e_q \rho \cos \Theta_{\text{cm}} + 1)^2}. \quad (42)$$

It is straightforward to show that in the massless limit ($\rho = 1$) Eq. (39) reduces to Eq. (28). Note that at the positions of the zeros we have, as in the massless case,

$$[12]_{m_q} = e_q^2 \left([34]_{m_q} - \frac{1}{2} \{ [33]_{m_q} + [44]_{m_q} \} \right), \quad (43)$$

with the interference again canceling the sum of these two terms.

Taken together, the equations (39–42) only have physical solutions for a certain range of $\rho \in [\rho_{\text{crit}}, 1]$. In particular, if the ratio m_q/E_{e^-} (quark mass over beam energy) becomes too large the radiation zeros disappear. Fig. 5 shows the positions $\hat{\theta}_\gamma$ of the radiation zeros inside the event plane ($\hat{\phi}_\gamma = 0^\circ$) as a function of ρ for a fixed beam energy $E_{e^-} = 100$ GeV, for both d -type and u -type quarks, and for different values of the c.m.s. scattering angle Θ_{cm} . The dashed lines indicate the values of ρ_{crit} . There is one kinematic configuration $\tilde{\Theta}_{\text{cm}}$ for which m_q^{crit} becomes maximal, i.e. an upper limit on the quark mass for which radiation zeros can still be observed. We find

$$\tilde{\rho}_{\text{crit}} = \frac{1}{2} \sqrt{4 - e_q^2} \iff \tilde{m}_q^{\text{crit}} = \frac{\sqrt{s} |e_q|}{2} \iff \cos \tilde{\Theta}_{\text{cm}} = \frac{-e_q}{\sqrt{4 - e_q^2}}. \quad (44)$$

For the production of d -type quarks we obtain $\widetilde{m}_q^{\text{crit}} = 16.7$ GeV at $\widetilde{\Theta}_{\text{cm}} = 80.3^\circ$, and for u -type quarks we find $\widetilde{m}_q^{\text{crit}} = 33.3$ GeV at $\widetilde{\Theta}_{\text{cm}} = 110.7^\circ$. According to Eq. (44) we require a beam energy of at least $E_{e^-} = 525$ GeV to observe radiation zeros in the process $e^-e^+ \rightarrow t\bar{t}\gamma$ assuming a top quark mass of $m_t = 175$ GeV and an even higher energy to achieve a reasonable separation from the outgoing partons (see Fig. 6).⁵

For $\Theta_{\text{cm}} = 90^\circ$ we can write the solutions in a very compact form. We find as a condition for which radiation zeros exist:

$$\rho \geq \rho_{\text{crit}} = \frac{2}{\sqrt{4 + e_q^2}} \iff m_q \leq \frac{\sqrt{s}}{2} \frac{|e_q|}{\sqrt{4 + e_q^2}}. \quad (45)$$

For example, in order to observe radiation zeros in 90° back-to-back scattering with $E_{e^-} = 100$ GeV we need $m_{d\text{-type}} < 16.4$ GeV or $m_{u\text{-type}} < 31.6$ GeV, conditions satisfied by all five light-quark flavours.

In Table 1 we present numerical values for ρ_{crit} and for m_q^{crit} , assuming a beam energy for the latter of $E_{e^-} = 100$ GeV. The values for ρ_{crit} are illustrated in Fig. 5.

Θ_{cm}	d -type quarks		u -type quarks	
	$\rho \geq$	$m_q \leq$	$\rho \geq$	$m_q \leq$
15°	0.9986	5.23 GeV	0.9977	6.72 GeV
30°	0.9951	9.82 GeV	0.9913	13.18 GeV
45°	0.9911	13.34 GeV	0.9815	19.13 GeV
60°	0.9878	15.60 GeV	0.9699	24.34 GeV
75°	0.9861	16.59 GeV	0.9583	28.58 GeV
90°	0.9864	16.44 GeV	0.9487	31.62 GeV

Table 1: Conditions for the appearance of radiation zeros for different c.m.s. frame scattering angles Θ_{cm} . The numbers in each row are ρ_{crit} and m_q^{crit} , assuming a beam energy of $E_{e^-} = 100$ GeV for the latter. Critical mass values for other beam energies can be obtained by simple rescaling.

An interesting conclusion from Table 1 concerns $e^-e^+ \rightarrow b\bar{b} + \gamma$. Assuming a mass for the b quark of $m_b \simeq 4.5$ GeV, the actual kinematics for the observation of radiation zeros become critical, especially at small c.m.s. scattering angles. For example, the outgoing b and \bar{b} jets should be located at around $90^\circ \pm 30^\circ$ from the beam direction (cf. Fig. 6). Then the radiation zeros not only exist, but are also reasonably well separated from the collinear singularities (again cf. Fig. 6).

⁵We do not consider here the contributions to the radiation pattern from photon emission off the decay products of heavy unstable quarks.

5 Radiation zeros for arbitrary photon energies

We have so far identified radiation zeros using analytic techniques in the soft-photon approximation to the scattering matrix elements and phase space. However, as for the $eq \rightarrow eq\gamma$ scattering process studied in Ref. [13], zeros are also found in the *exact* cross section for fixed photon energies up to a critical maximum value.

To quantify this, we study planar $e^-e^+ \rightarrow q\bar{q}\gamma$ events in which (i) the polar angle of the quark (Θ_{cm}) is fixed, (ii) the energy of the photon (ω_γ) is fixed, and (iii) the polar angle of the photon (θ_γ) is varied. Note that the energy of the quark and the four-momentum of the antiquark are then fixed by energy-momentum conservation. In the limit $\omega_\gamma \rightarrow 0$ the kinematics of the soft-photon approximation studied in previous sections are reproduced. We find, as in Ref. [13], that the matrix element has radiation zeros for non-zero ω_γ , and that the position of the zero varies smoothly as ω_γ increases from zero. This is illustrated in Fig. 7, which shows the position $\hat{\theta}_\gamma$ of the zero as a function of ω_γ , for d -type and u -type quarks and $\Theta_{\text{cm}} = 90^\circ$. The values at $\omega_\gamma = 0$ coincide with those obtained analytically in the soft-photon approximation, see for example Fig. 4. A variation of the position of the zero with the photon energy is to be expected, since with the above kinematics the direction of the antiquark changes as the photon energy is varied.

If the photon is too energetic then the zeros can disappear. This was also a feature of the $eq \rightarrow eq\gamma$ process studied in Ref. [13]. For example, for $e_q = +2/3$ and $\Theta_{\text{cm}} = 90^\circ$ we only have radiation zeros for $\omega_\gamma/E_{\text{beam}} < 0.47$. However because of the soft-photon energy spectrum, such upper limits are not particularly relevant in practice. Since the position of the zero varies with the photon energy, any binning in this quantity (above say some small threshold value $\omega_\gamma^{\text{min}}$) will remove the zero and replace it with a sharp minimum located near the corresponding soft-photon approximation position. We will illustrate this in the following section.

6 A Monte Carlo study for $b\bar{b}\gamma$ production

Our study so far has been based on the ideal but unrealistic situation of well-defined four-momenta for the jets and the photon, fixed at particular directions in phase space. In practice, experiments deal with binned quantities and jets of finite mass and width. A more realistic study should therefore take these into account. Rather than try to model a particular detector capability, we can define a simple set of cuts which should take the main effects of smearing and binning into account. The aim is to see whether the radiation zeros remain visible after a more realistic analysis. We will, however, make the assumption that in our sample of $b\bar{b}\gamma$ events the b -jet can be distinguished from the \bar{b} -jet. This guarantees a radiation zero in the ideal case, as discussed in the previous sections.

We first generate a sample of $b\bar{b}\gamma$ events using a Monte Carlo which includes the exact phase space and matrix element. We choose a centre-of-mass energy of $\sqrt{s} = 200$ GeV. For this energy we can safely use the $m_b = 0$ massless quark approximation. As a further simplification we include only s -channel γ^* exchange.⁶ The following sequence of cuts is

⁶Including also Z exchange only affects the overall normalisation and not the shape of the photon distributions.

applied:

$$10 \text{ GeV} < \omega_\gamma < 40 \text{ GeV} < E_{\bar{b}} < E_b , \quad (46)$$

to ensure that the photon is the softest particle in the final state, and that the b -quark direction coincides with the thrust axis of the event. The photon is also required to be separated in angle from the beam and jet directions:

$$\theta_{\gamma,\text{beam}} > 20^\circ , \quad \theta_{\gamma,b}\theta_{\gamma,\bar{b}} > 10^\circ . \quad (47)$$

These cuts serve to define a ‘measurable’ sample of $b\bar{b}\gamma$ events.

To investigate the radiation zero we must introduce a planarity cut on the $b\bar{b}\gamma$ final state. We do this by requiring that the normals to the two planes defined by (i) the beam and outgoing b -quark directions and (ii) the \bar{b} -quark and photon directions are approximately parallel:

$$|\vec{n}_{13} \cdot \vec{n}_{4k}| > \cos 20^\circ , \quad (48)$$

using the notation for momenta defined in Eq. (7). We can then study the polar angle (θ_γ) distribution of the photon for various values of the polar angle (Θ_{cm}) of the thrust axis (b -quark direction) with respect to the beam direction. In practice, we consider a bin centred on $\theta_b = \Theta_{\text{cm}}$ of width 10° , i.e. we integrate over

$$\Theta_{\text{cm}} - 5^\circ < \theta_b < \Theta_{\text{cm}} + 5^\circ . \quad (49)$$

Note that our cuts are deliberately chosen to mimic the soft-photon kinematics used in Section 2. However because we integrate over the photon energy and smear the polar angle and planarity criteria we expect to see *dips* in the photon distribution rather than strict zeros.

Figure 8 shows the θ_γ distribution for (a) $\Theta_{\text{cm}} = 60^\circ$, (b) $\Theta_{\text{cm}} = 90^\circ$ and (c) $\Theta_{\text{cm}} = 120^\circ$. Comparing with Fig. 2, we once again see sharp dips at approximately the same position as in the ‘ideal’ soft-photon case. Note that the collinear singularities evident in Fig. 2 are now removed by the cuts. The suppression of the cross section at the position of the zeros can further be appreciated by comparing with the results obtained when the interference term in the matrix element squared is set to zero, corresponding to incoherent photon emission off the initial and final states. The results of this approximate calculation, shown as dashed lines in Fig. 8, do not exhibit any dip structure in the region of the zeros and are clearly distinguishable from the exact results.

7 Conclusions

Radiation zeros are an important consequence of the gauge structure of the electromagnetic interaction. They arise in different types of high-energy scattering processes. In this paper we have investigated a particular type of radiation zero (‘type 2’ or ‘planar’) which is a feature of the process $e^+e^- \rightarrow q\bar{q}\gamma$. We derived expressions for the locations of the zeros in the soft-photon limit, and showed that the zeros persist for hard photons and massive quarks. However the experimental verification of such zeros is not straightforward. The zeros disappear on the Z^0 pole because the interference between initial- and final-state radiation is suppressed by the finite Z lifetime. The collision energy must therefore be greater or less

than M_Z . Unfortunately the number of events beyond the Z^0 pole at present colliders is quite low. Apart from the resulting issue of the overall event rate, it is necessary to be able to distinguish quark from antiquark jets in order to compare with our predictions. This can perhaps be done with some efficiency for b -quark jets. We performed a Monte Carlo study which showed that ‘realistic’ distributions do indeed exhibit sharp dips in particular regions of phase space. Further studies using a more complete simulation of the final-state hadronisation process would be worthwhile.

Acknowledgements

We are grateful to Z. Wąs for discussions on Z^0 pole radiation and J. Turnau for some helpful remarks. MH wishes to thank the members of the *H. Niewodniczański Institute of Nuclear Physics* (Kraków) for their hospitality during the final stages of this work and also gratefully acknowledges financial support in the form of a DAAD–Doktorandenstipendium (HSP III).

References

- [1] R.W. Brown, talk presented at the International Symposium on Vector–Boson Self–Interactions, February 1995, Los Angeles (UCLA), hep-ph/9506018.
- [2] K.O. Mikaelian, D. Sahdev and M.A. Samuel, *Phys. Rev. Lett.* **43** (1979) 746.
- [3] R.W. Brown, D. Sahdev and K.O. Mikaelian, *Phys. Rev.* **20** (1979) 1164.
- [4] D. Benjamin for the CDF Collaboration, Proc. 10th Topical Workshop on Proton–Antiproton Collider Physics, Fermi National Accelerator Laboratory, Batavia, IL, May 9–13, 1995, preprint FERMILAB–CONF–95/241–E (1995).
- [5] S.J. Brodsky and R.W. Brown, *Phys. Rev. Lett.* **49** (1982) 966.
S.J. Brodsky, R.W. Brown and K.L. Kowalski, *Phys. Rev.* **D28** (1983) 624.
G. Passarino, *Nucl. Phys.* **B224** (1983) 265.
M.L. Laursen, M.A. Samuel and A. Sen, *Phys. Rev.* **D28** (1983) 650.
M.L. Laursen, M.A. Samuel, A. Sen and G.S. Sylvester, *Phys. Rev.* **D29** (1984) 994.
M.L. Laursen, M.A. Samuel, A. Sen and G.S. Sylvester, *Phys. Rev.* **D31** (1985) 1657.
- [6] U. Baur, T. Han and J. Ohnemus, *Phys. Rev. Lett.* **72** (1994) 3941.
- [7] U. Baur, T. Han, N. Kauer, R. Sobey and D. Zeppenfeld, *Phys. Rev.* **D56** (1997) 140.
- [8] T. Abraha and M.A. Samuel, Oklahoma State U. preprint OSU–RN–326, hep-ph/9706336.
- [9] C.L. Bilchak, *J. Phys.* **G11** (1985) 1117.
- [10] G. Couture, *Phys. Rev.* **D39** (1989) 2527.
- [11] G. Li, J. Reid and M.A. Samuel, *Phys. Rev.* **D41** (1990) 1675.
- [12] M.A. Doncheski and F. Halzen, *Z. Phys.* **C52** (1991) 673.
- [13] M. Heyssler and W.J. Stirling, Durham preprint DTP/97/66, *Z. Phys.* (in press), hep-ph/9707373.
- [14] F.A. Berends, R. Kleiss, P. De Causmaecker, R. Gastmans and T.T. Wu, *Phys. Lett.* **B103** (1981) 124.
- [15] Yu.L. Dokshitzer, V.A. Khoze and S.I. Troyan, in Proc. 6th Int. Conf. on Physics in Collision, ed. M. Derrick (World Scientific, Singapore, 1987), p.417.
Yu.L. Dokshitzer, V.A. Khoze and S.I. Troyan, *Sov. J. Nucl. Phys.* **46** (1987) 712.
- [16] Yu.L. Dokshitzer, V.A. Khoze, A.H. Mueller and S.I. Troyan, *Rev. Mod. Phys.* **60** (1988) 373.
Yu.L. Dokshitzer, V.A. Khoze and S.I. Troyan in: Advanced Series on Directions in High Energy Physics, Perturbative Quantum Chromodynamics, ed. A.H. Mueller (World Scientific, Singapore), v. 5 (1989) 241.

- [17] Yu.L. Dokshitzer, V.A. Khoze, A.H. Mueller and S.I. Troyan, “Basics of Perturbative QCD”, ed. J. Tran Thanh Van, Editions Frontières, Gif-sur-Yvette, 1991.
- [18] G. Jikia, *Phys. Lett.* **B257** (1991) 196.
- [19] Yu.L. Dokshitzer, V.A. Khoze and S.I. Troyan, University of Lund preprint LU-TP-92-10 (1992).
- [20] V.A. Khoze, L.H. Orr and W.J. Stirling, *Nucl. Phys.* **B378** (1992) 413.
- [21] Yu.L. Dokshitzer, V.A. Khoze, L.H. Orr and W.J. Stirling, *Nucl. Phys.* **B403** (1993) 65.
- [22] V.A. Khoze, J. Ohnemus and W.J. Stirling, *Phys. Rev.* **D79** (1994) 1237.
- [23] S. Jadach and Z. Was, *Phys. Lett.* **B219** (1989) 103; preprint CERN-TH 7232/94 (1994).
- [24] DELPHI collaboration: P. Abreu *et al.*, *Z. Phys.* **C72** (1996) 31.

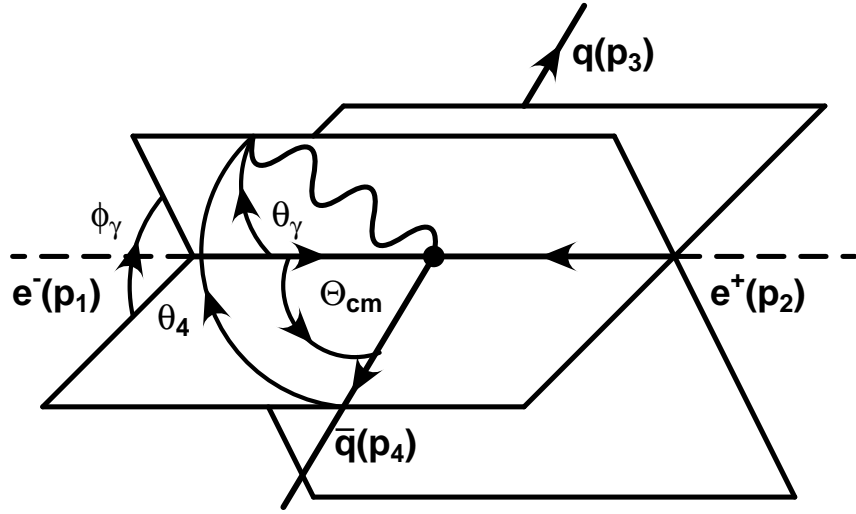


Figure 1: Parameterisation of the kinematics for $e^-(p_1)e^+(p_2) \rightarrow q(p_3)\bar{q}(p_4)+\gamma(k)$ scattering in the e^-e^+ c.m.s. frame. The orientation of the photon relative to the scattering plane is denoted by the angles θ_γ and ϕ_γ . Note that $\theta_\gamma = \theta_2$.

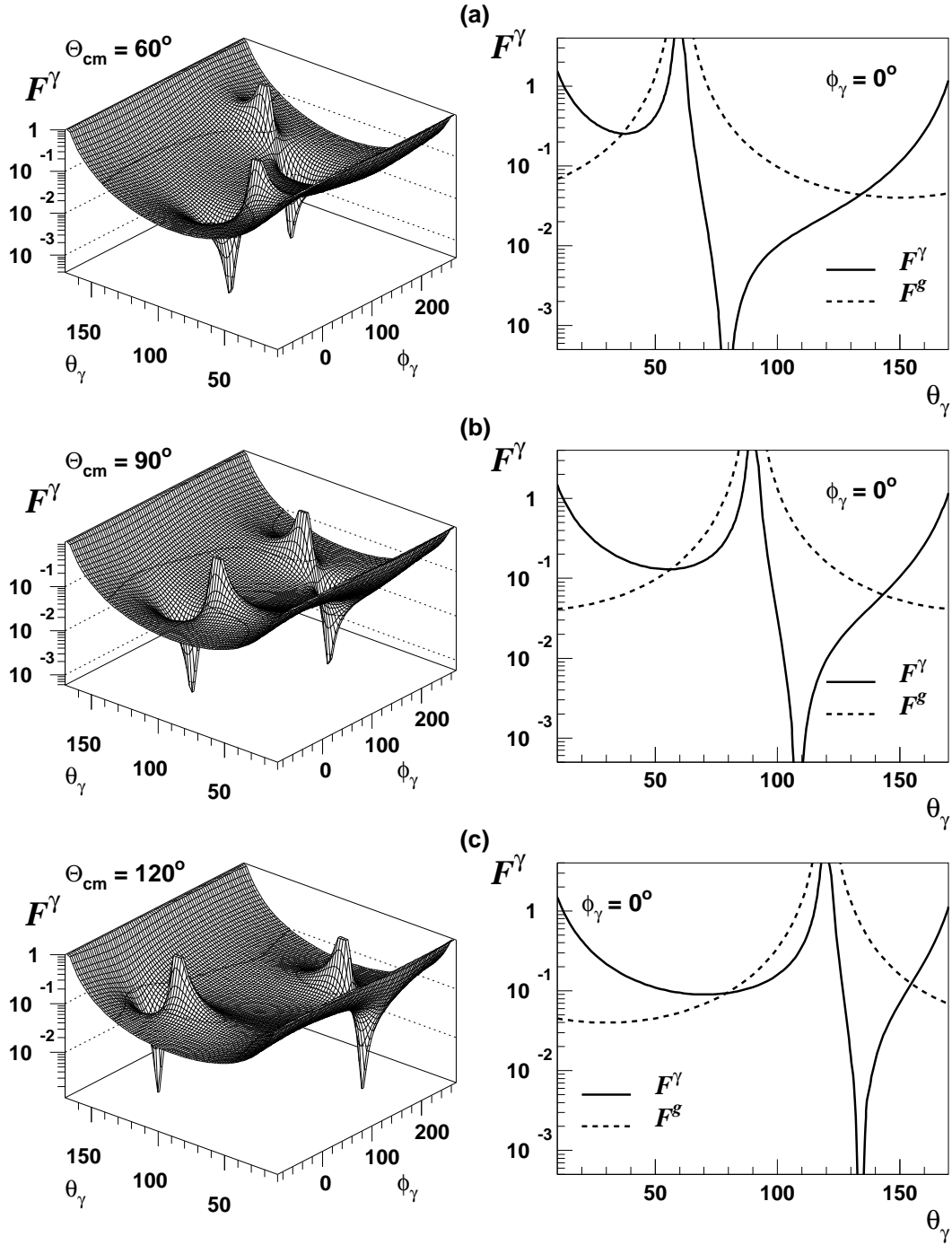


Figure 2: Surface plots of the antenna pattern \mathcal{F}^γ in the angular phase space of the soft photon (left-hand side) and slices through the event plane (right-hand side) at $\hat{\phi}_\gamma = 0^\circ$ to illustrate the positions of the radiation zeros. We show the process $e^-e^+ \rightarrow q_d\bar{q}_d\gamma$ for three different c.m.s. frame angles (a) $\Theta_{\text{cm}} = 60^\circ$, (b) $\Theta_{\text{cm}} = 90^\circ$ and (c) $\Theta_{\text{cm}} = 120^\circ$. The dashed lines are the corresponding distributions for soft gluon emission.

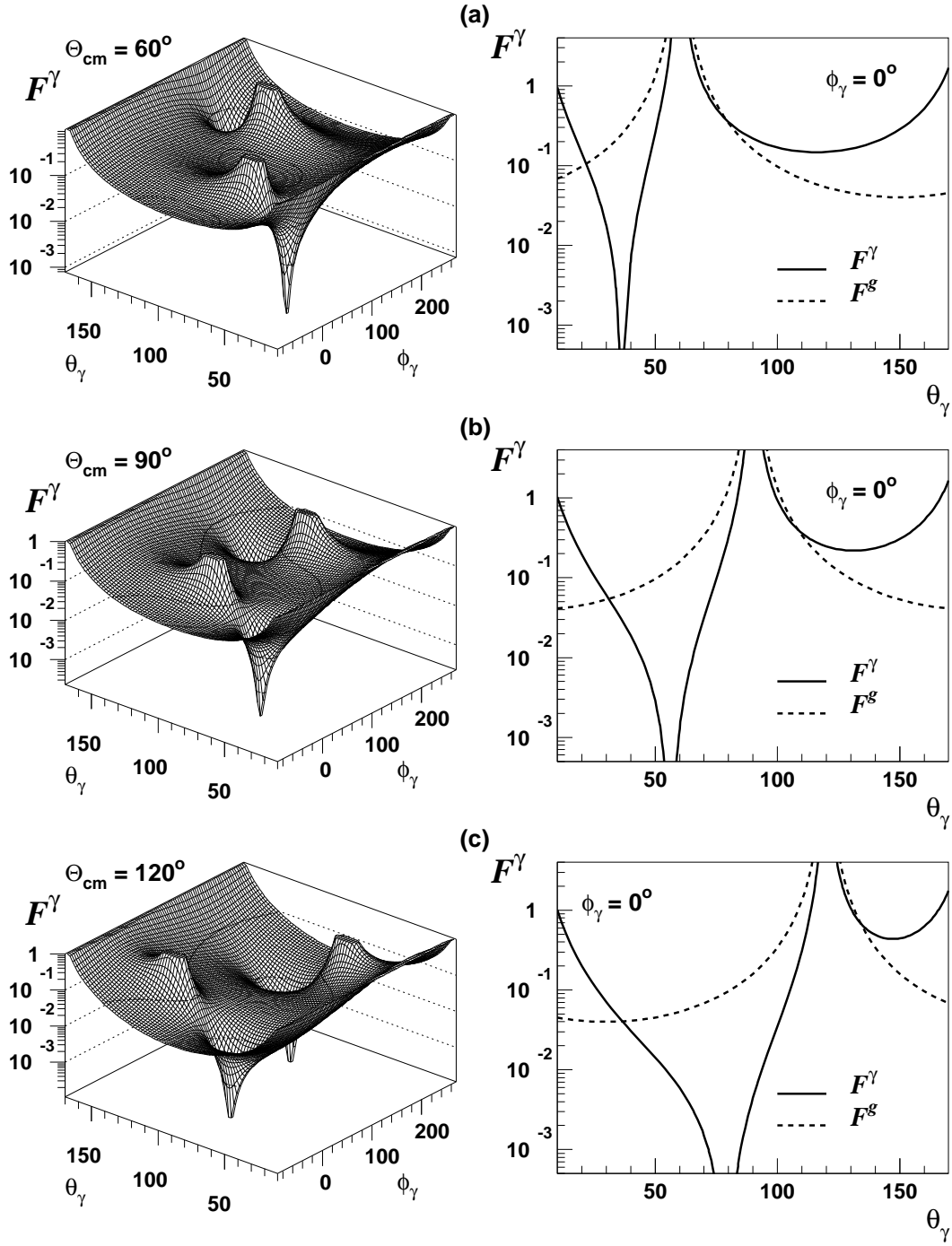


Figure 3: Same as Fig. 2, but for the process $e^-e^+ \rightarrow q_u\bar{q}_u\gamma$.

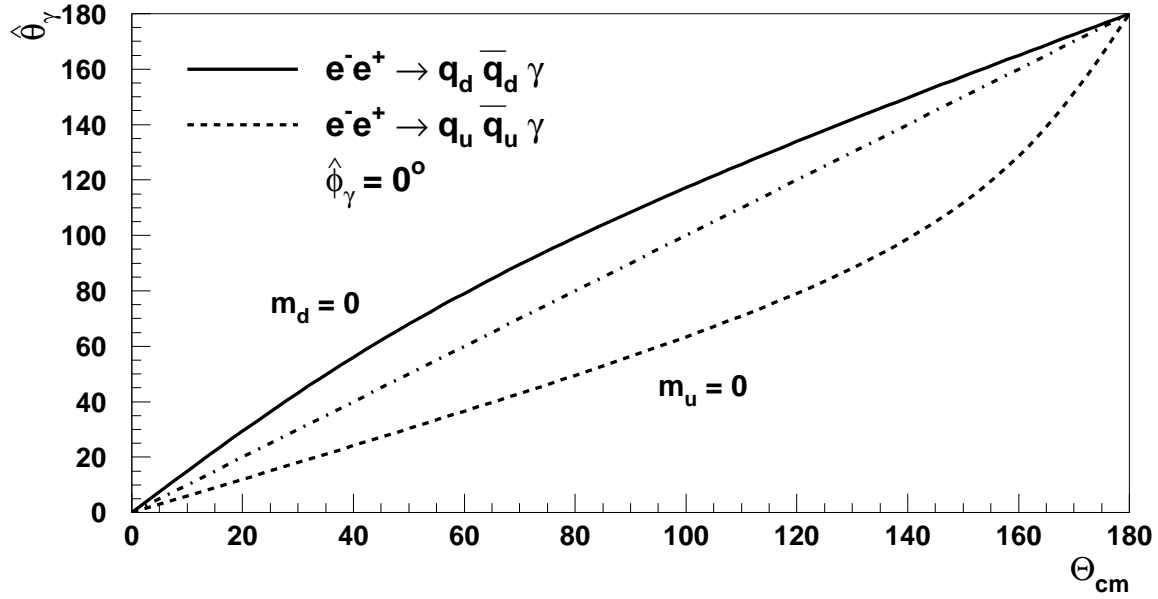


Figure 4: The positions $(\hat{\phi}_\gamma, \hat{\theta}_\gamma)$ of the radiation zeros for the processes $e^-e^+ \rightarrow q_d \bar{q}_d \gamma$ and $e^-e^+ \rightarrow q_u \bar{q}_u \gamma$ as a function of the c.m.s. frame scattering angle Θ_{cm} and fixed $\hat{\phi}_\gamma = 0^\circ$. The dot-dashed line shows the position of the final-state collinear singularity (i.e. the direction of the outgoing antiquark). Massless quarks are assumed. Note that the distribution for $\hat{\phi}_\gamma = 180^\circ$ shows a $\pi - \Theta_{\text{cm}}$ symmetry.

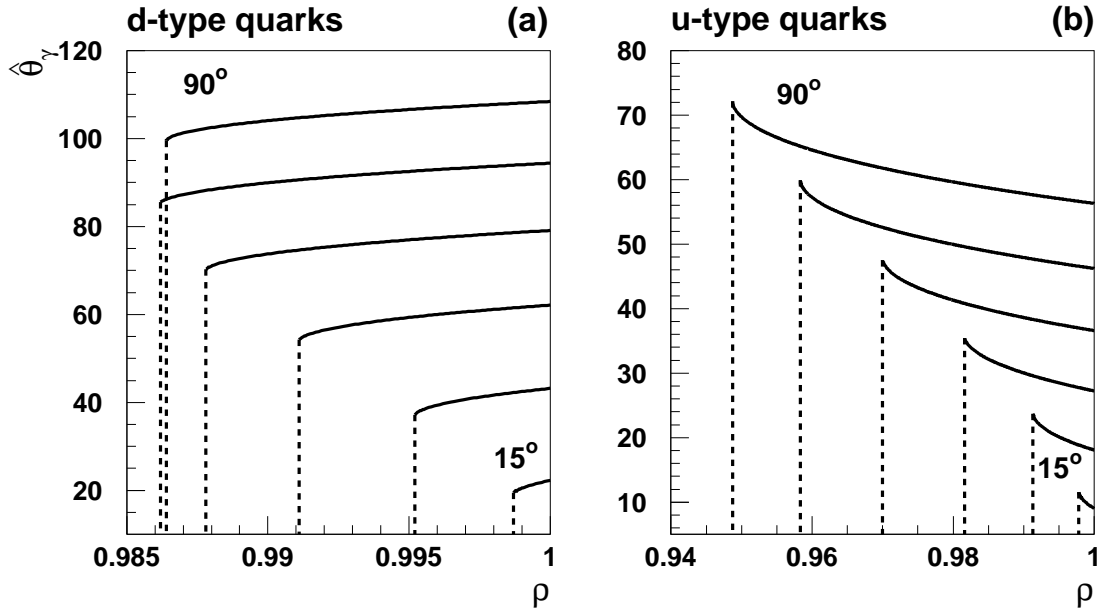


Figure 5: The positions of the radiation zeros $(\hat{\phi}_\gamma = 0^\circ, \hat{\theta}_\gamma)$ for massive quarks $\rho = \sqrt{1 - 4m_q^2/s}$ (beam energy $E_{e^-} = 100$ GeV) and different c.m.s. scattering angles ($\Theta_{\text{cm}} = 15^\circ - 90^\circ, \Delta\Theta_{\text{cm}} = 15^\circ$). The dashed lines show the values of ρ_{crit} .

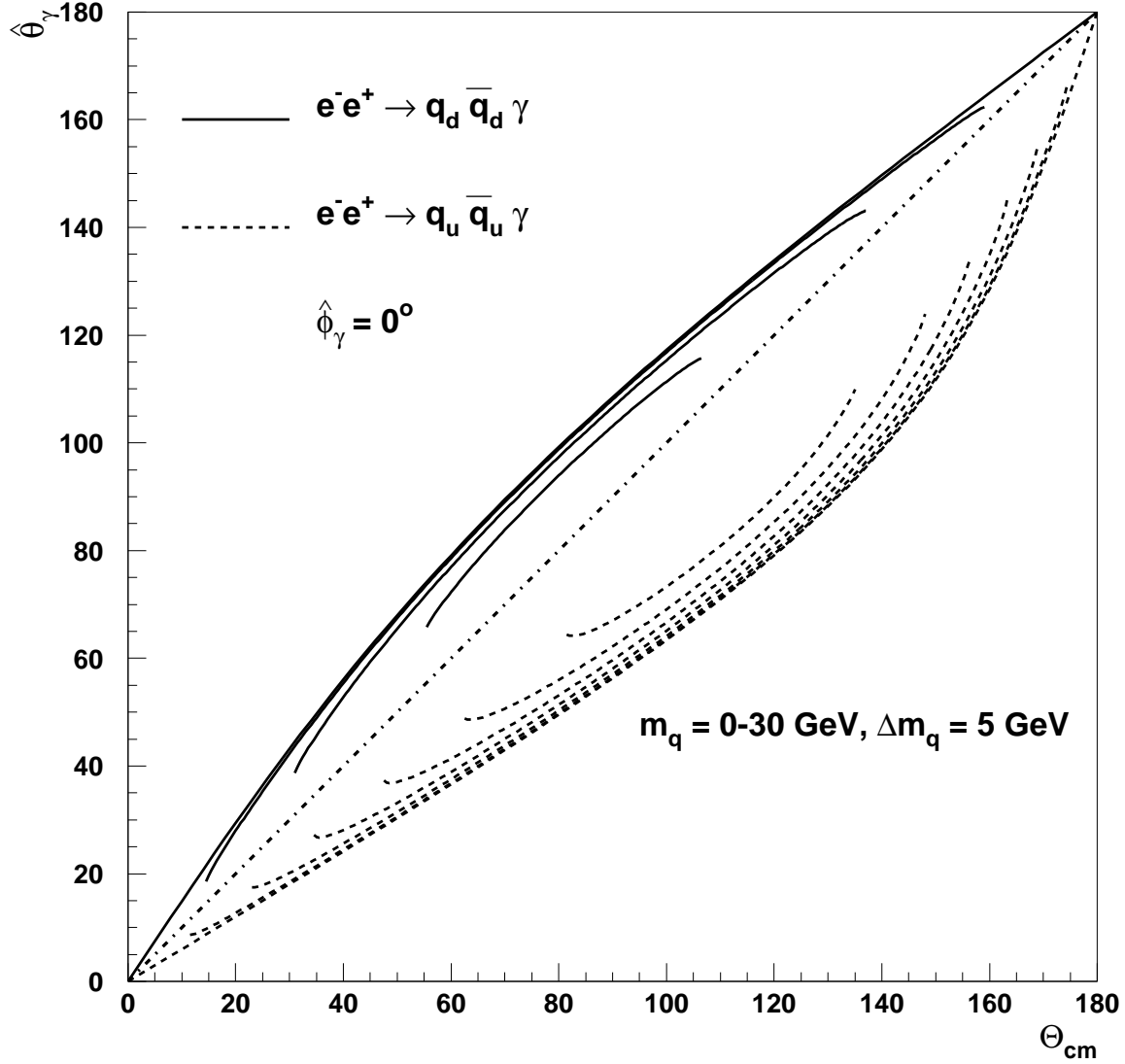


Figure 6: Same as Fig. 4 but now for massive quarks. The mass of the quarks is increased from $m_q = 0$ GeV to $m_q = 30$ GeV in steps of $\Delta m_q = 5$ GeV. The higher the mass the closer the positions of the zeros move towards the collinear singularity (dash-dotted line). The beam energy is $E_{e^-} = \sqrt{s}/2 = 100$ GeV. Note that the appearance of radiation zeros is dependent on the quark mass and the c.m.s. scattering angle Θ_{cm} .

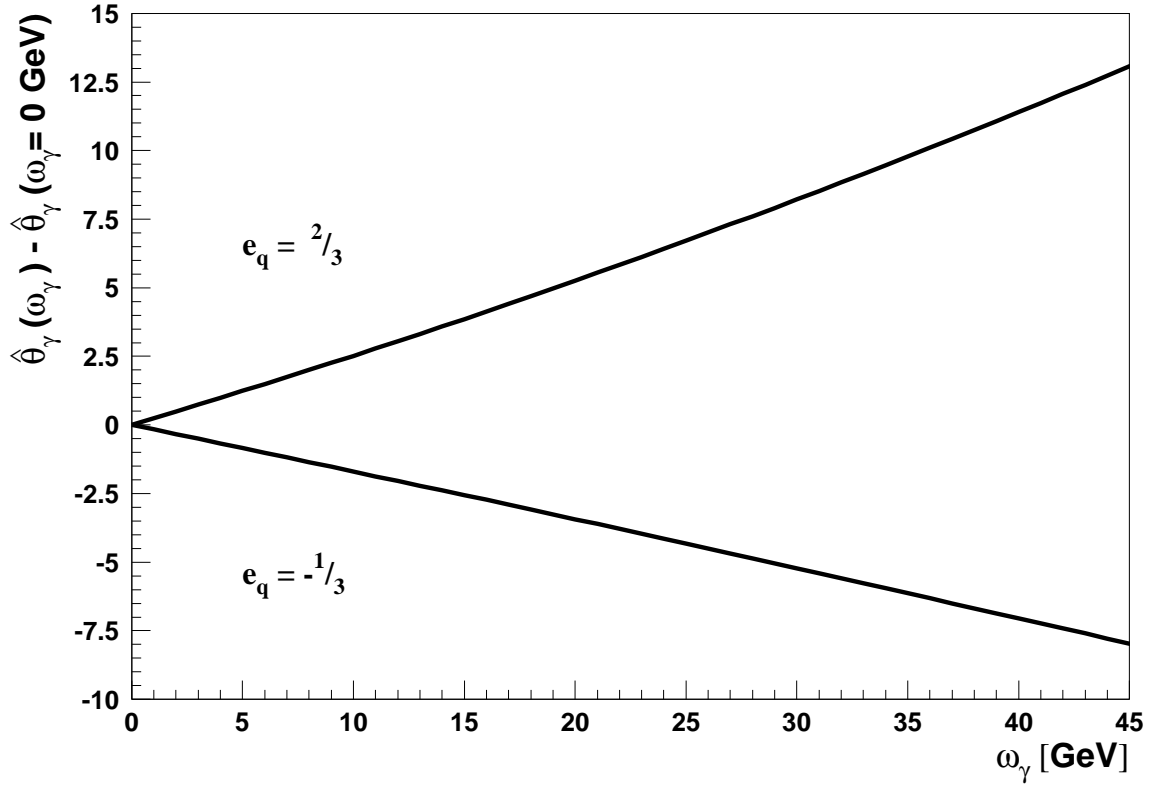


Figure 7: The positions $\hat{\theta}_\gamma$ of the radiation zeros for the processes $e^-e^+ \rightarrow qd\bar{q}d\gamma$ and $e^-e^+ \rightarrow qu\bar{q}u\gamma$ as a function of the photon energy ω_γ , for $E_{e^-} = \sqrt{s}/2 = 100$ GeV and fixed c.m.s. frame (quark) scattering angle $\Theta_{\text{cm}} = 90^\circ$.

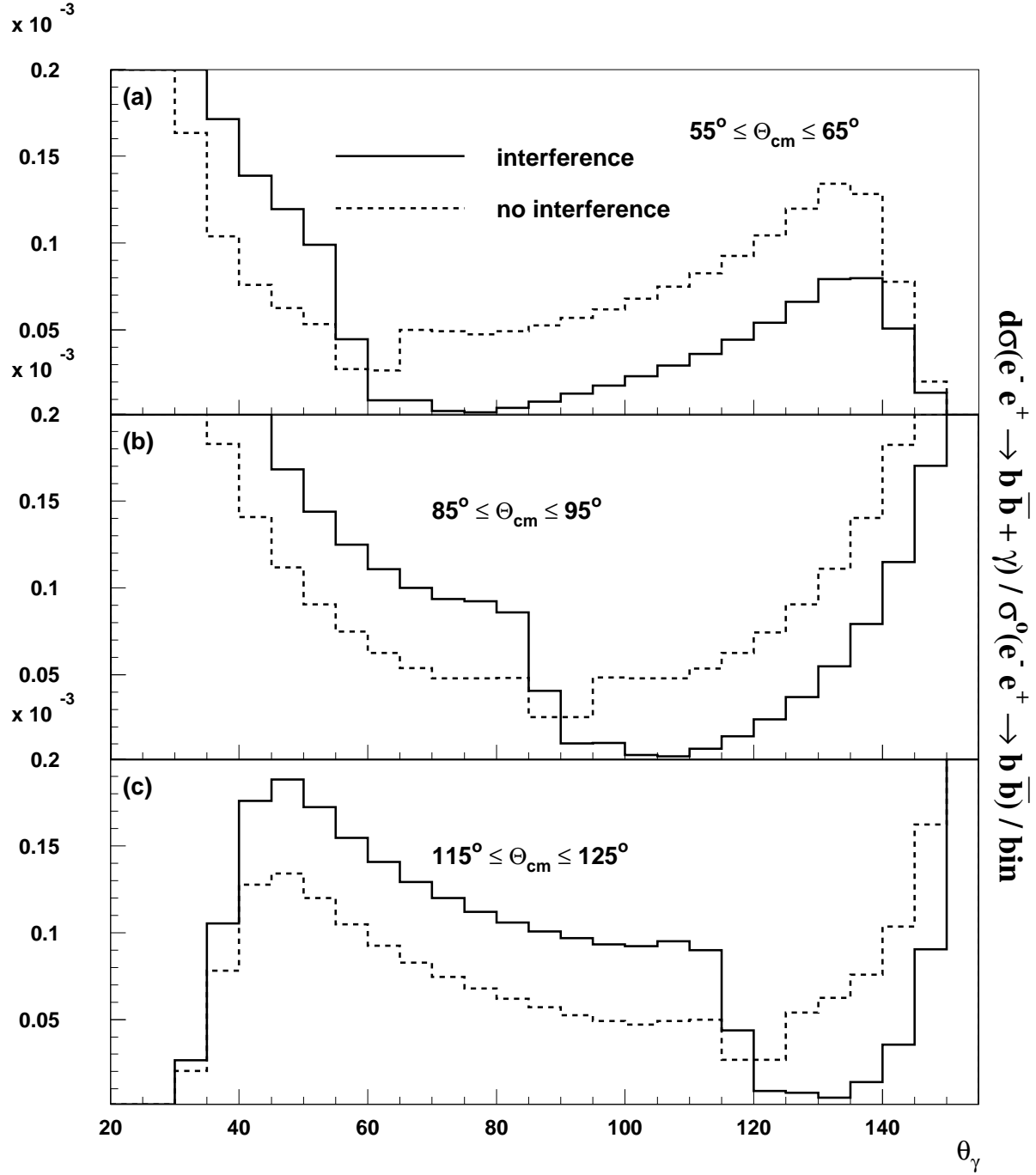


Figure 8: The θ_γ distribution (solid histograms) obtained in the Monte Carlo calculation of $e^-e^+ \rightarrow b\bar{b}\gamma$ in the planar configuration. The various cuts are defined in the text. The Θ_{cm} angles are (a) 60° , (b) 90° and (c) 120° . The dashed lines are the results of the corresponding calculation with the interference terms removed.